Supporting Information

Governing the morphology of Pt-Au heteronanocrystals with improved electrocatalytic performance

Stefanos Mourdikoudis,[a,b] Mariana Chirea,[a] Daniele Zanaga,[c] Thomas Altantzis,[c] Manasis Mitrakas,[b] Sara Bals,[c] Luis M. Liz-Marzán,[a,d,e] Jorge Pérez-Juste[a]* and Isabel Pastoriza-Santos[a]*

a Departamento de Química Física, CINBIO, Universidade de Vigo, 36310 Vigo, Spain

b Analytical Chemistry Laboratory, Department of Chemical Engineering, Aristotle University of Thessaloniki, 54124 Thessaloniki, Greece

c EMAT, University of Antwerp, Groenenborgerlaan 171, B-2020 Antwerp, Belgium

d Bionanoplasmonics Laboratory, CIC biomaGUNE, Paseo de Miramon 182, 20009 Donostia-San Sebastian, Spain

e Ikerbasque, Basque Foundation for Science, 48013 Bilbao, Spain

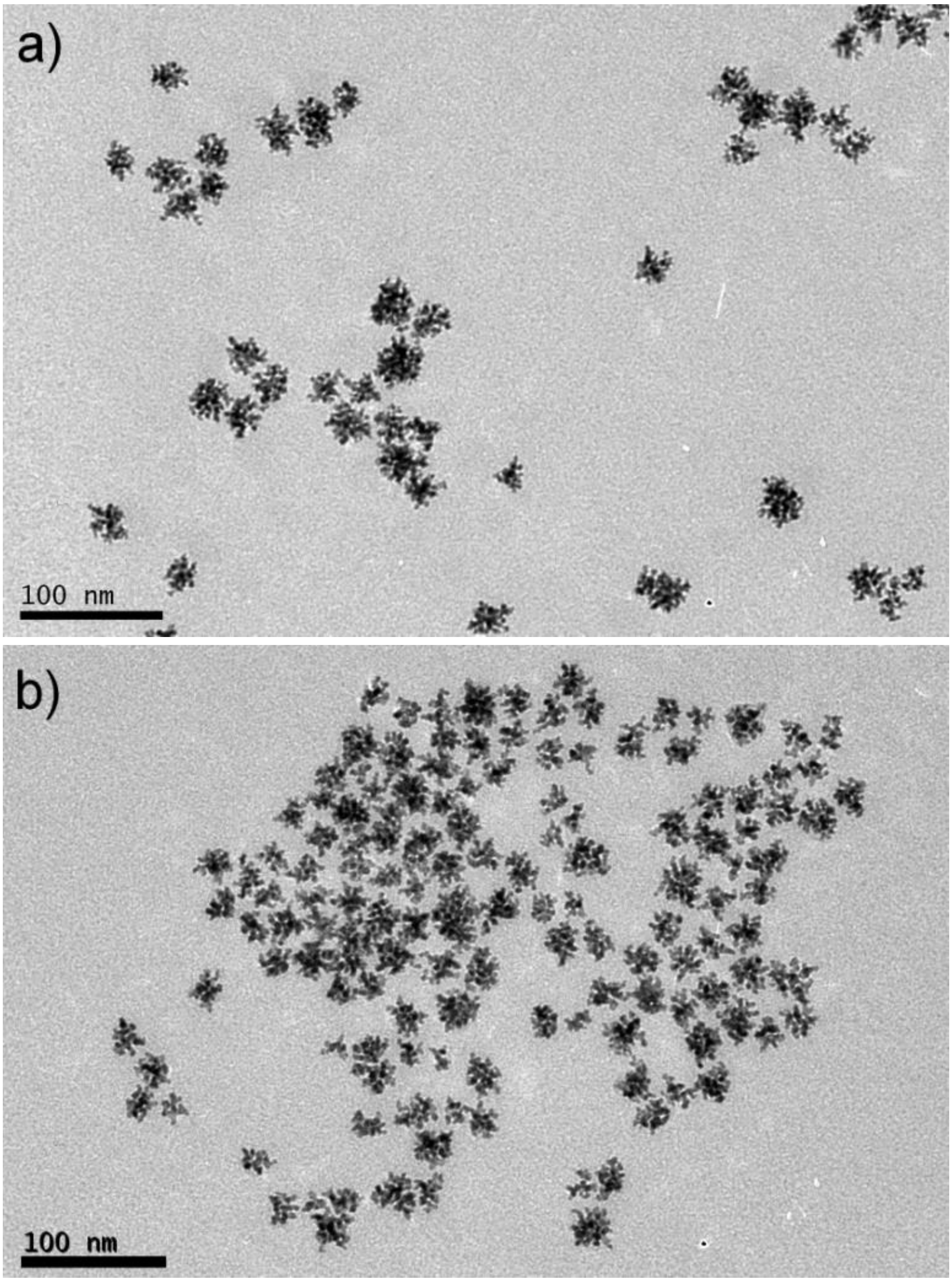

Fig. S1. Representative TEM images of Pt nanodendrites with different porosities; a) ‘medium-compact’ and b) porous.

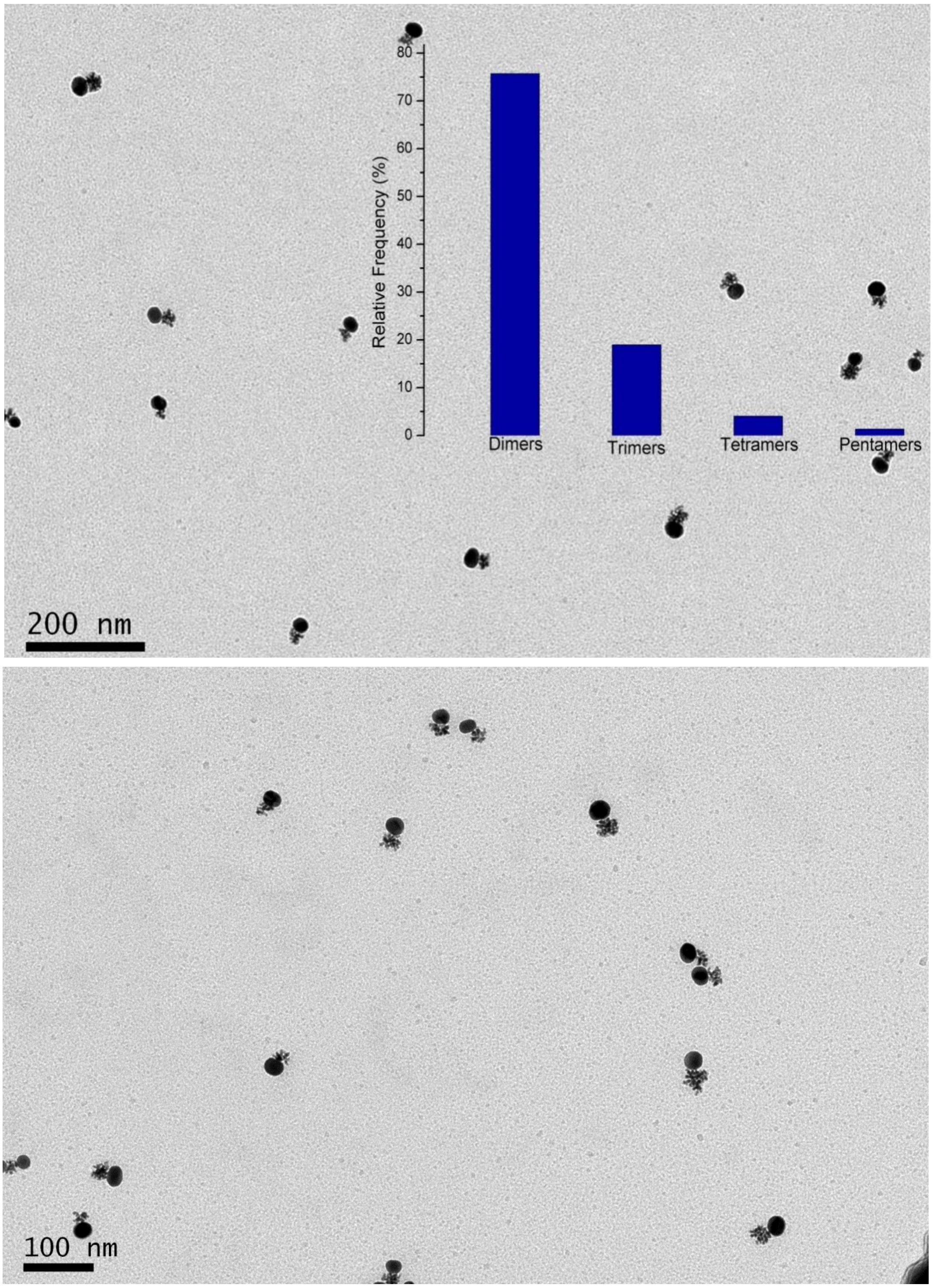

Fig. S2. Additional TEM images of Pt-Au dimers. (Inset) Histogram showing the relative distribution of Pt-Au multimers.

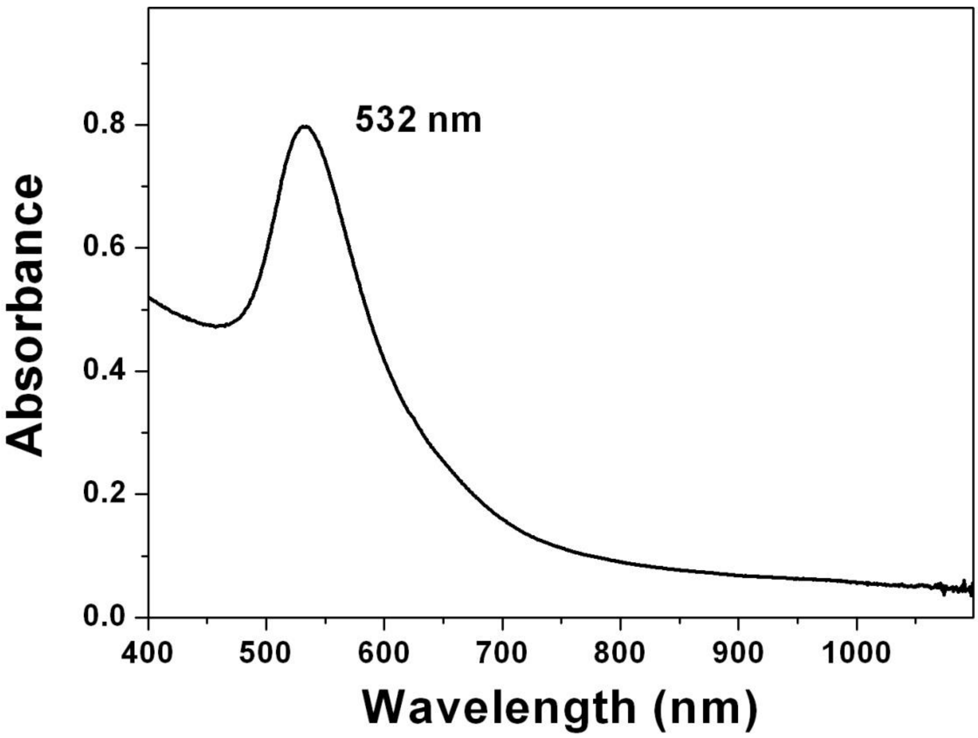

Fig. S3: Representative Vis-NIR extinction spectrum of an aqueous Pt-Au dimer colloidal dispersion. (Au particle size: 20 nm).

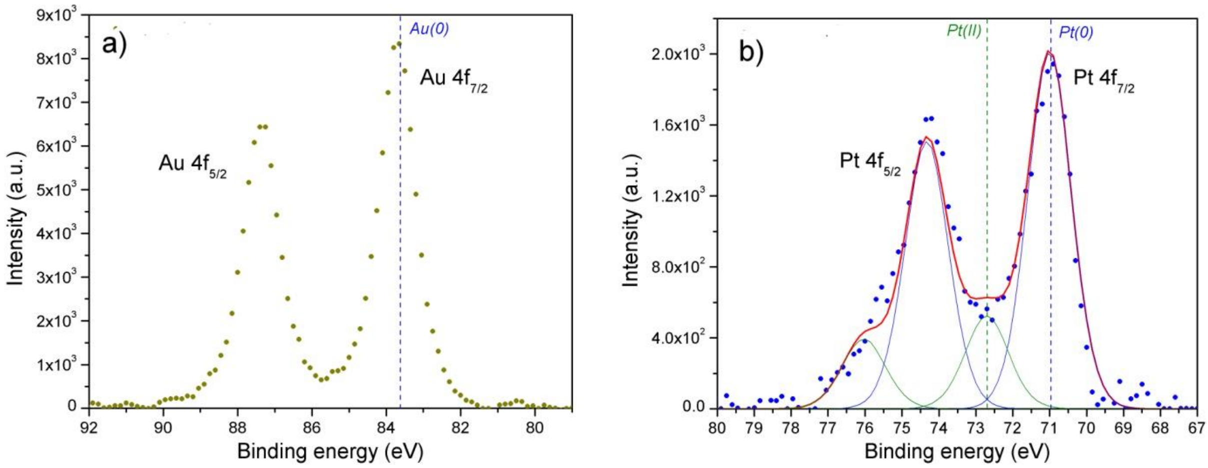

Fig. S4. High resolution XPS spectra for Au4f (a) and Pt4f (b) regions of the Pt-Au dimers showed in Fig. 1 of the main manuscript,.

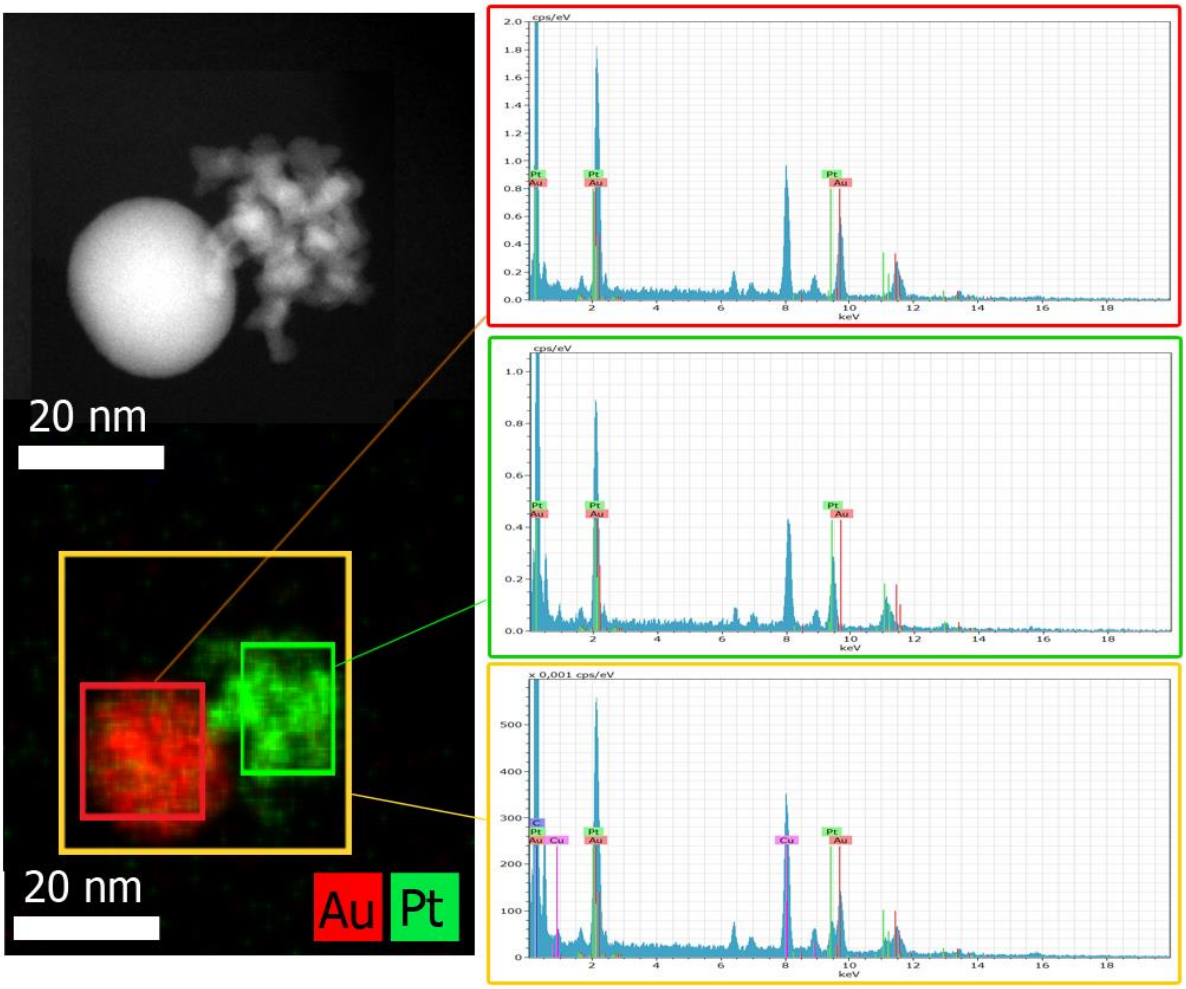

Fig. S5: HAADF image, EDX map and relative spectra of a Pt-Au dimer.

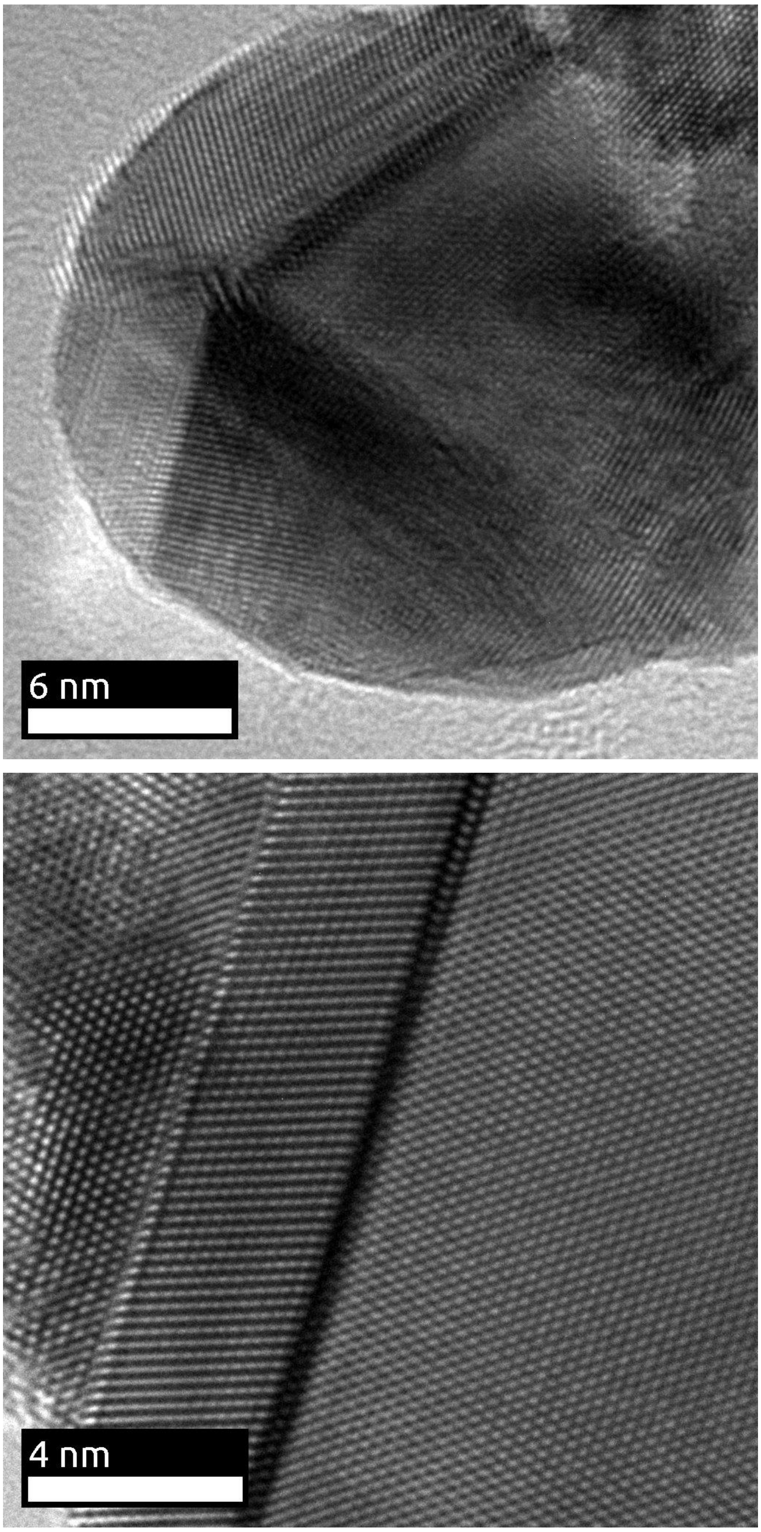

Fig. S6: HRTEM images of the gold particle shown in Figure 1c, revealing the existence of twinning.

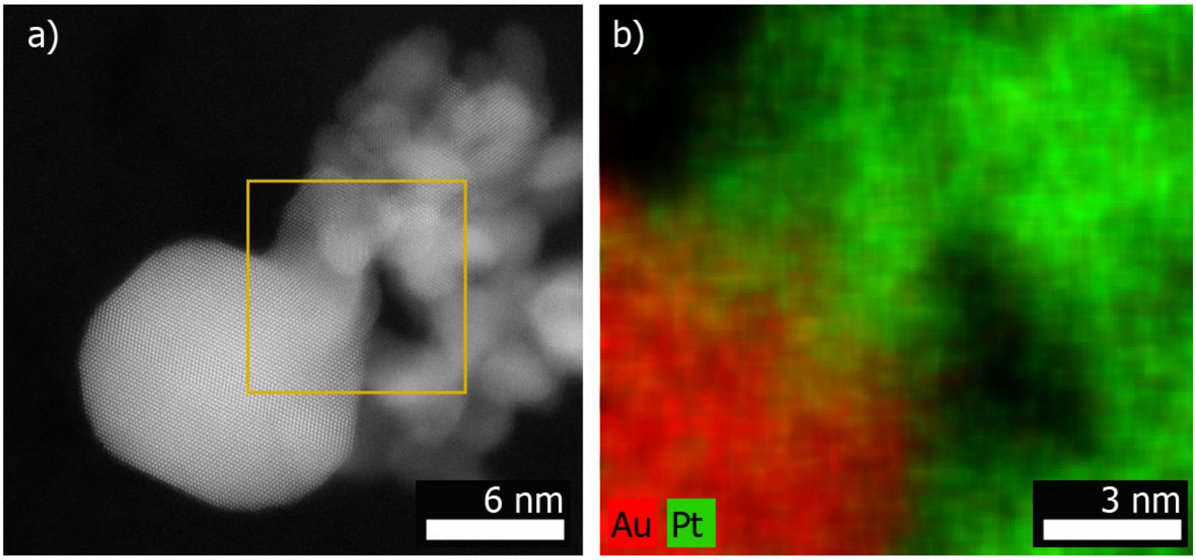

Fig. S7: (a) High resolution HAADF-STEM image acquired perpendicular to the interface between the gold particle and the platinum dendrite. b) EDX map of the zone in the yellow square of (a).

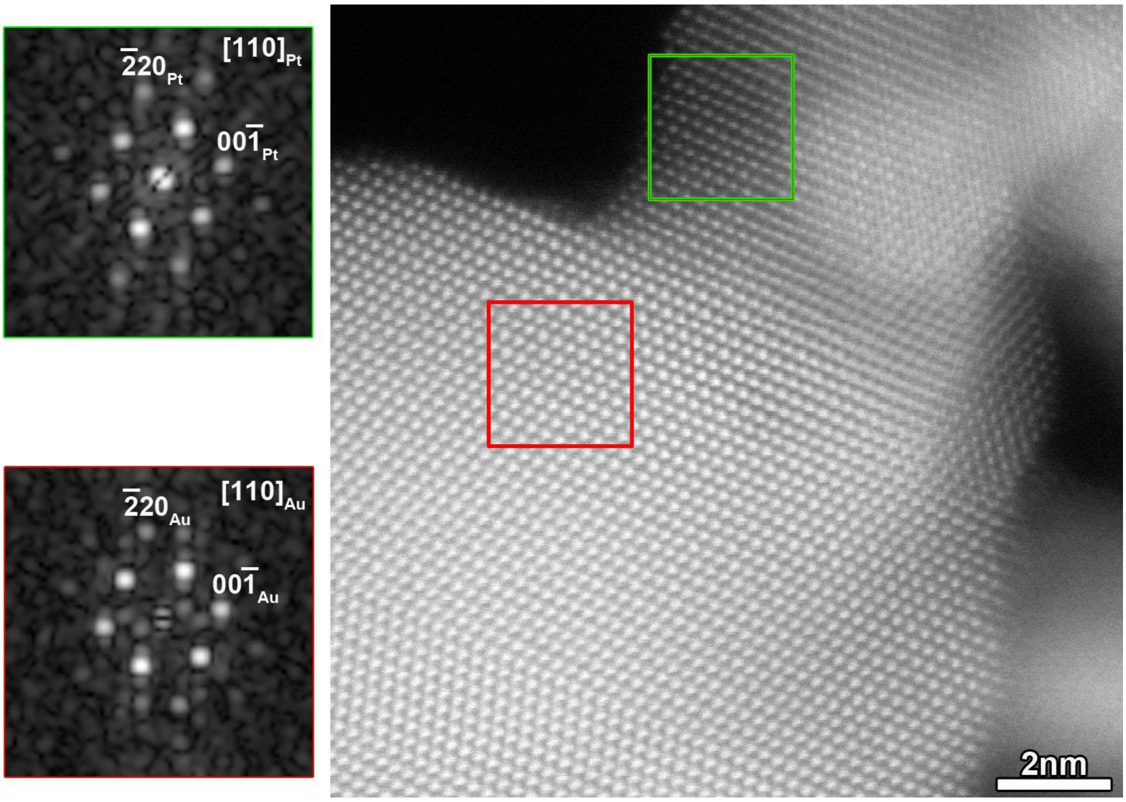

Fig. S8: Higher magnification of the zone in the yellow square of figure S6a. The FFT of the green region corresponds to Pt and that of the red square belongs to Au.

Table S1: Theoretical (Th) and experimental (Ex) values for the *d*-spacing for Au and Pt. The difference between these values verifies the epitaxial growth of Au on Pt.

Facet	Th. *d*-spacing (Å)		Ex. *d*-spacing (Å)		Difference %	
	Au	**Pt**	**Au**	**Pt**	**Au**	**Pt**
111	2.355	2.265	2.320	2.270	1.48	0.22
200	2.039	1.9616	2.050	1.960	0.54	0.08
220	1.442	1.3873	1.420	1.390	1.52	0.19

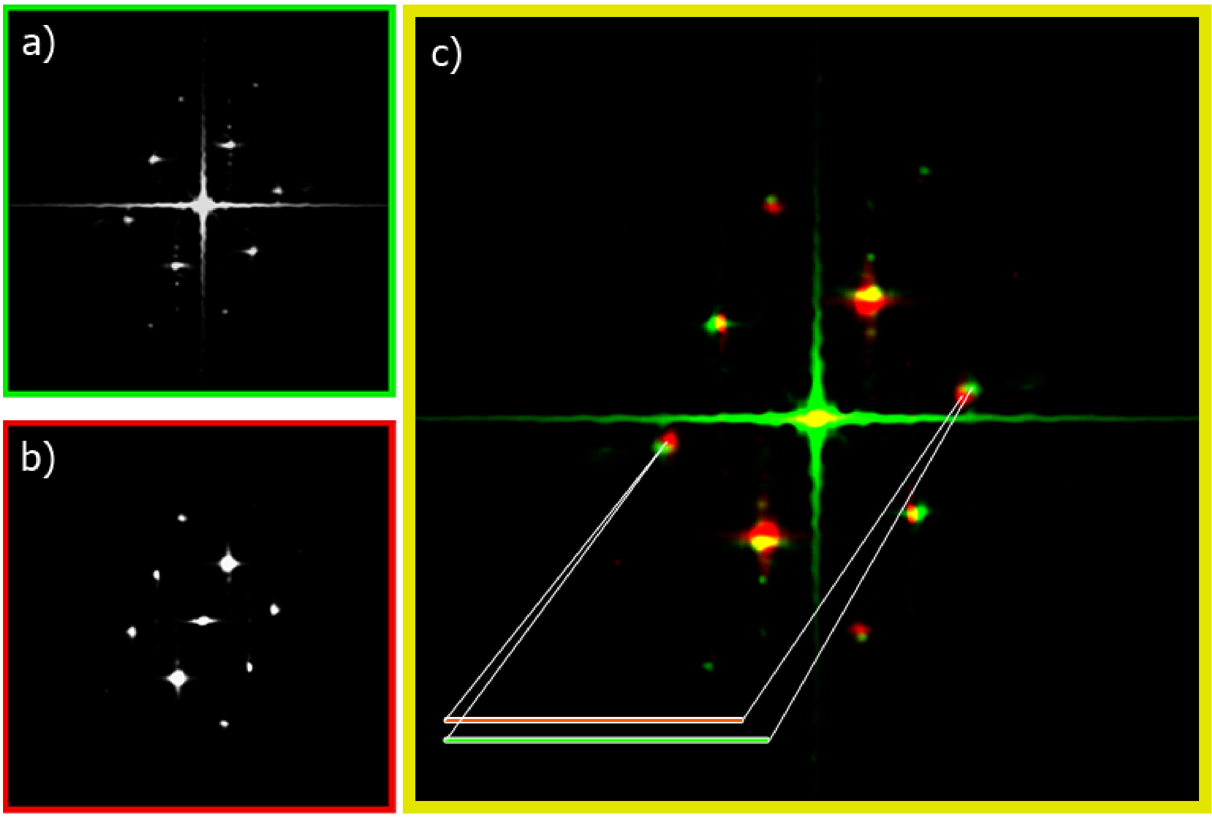

Fig. S9: FFTs of Pt zone (a) and Au zone (b), overlapped in c) to show the difference reflecting the bigger lattice parameters of Au (smaller distances between relative red dots).

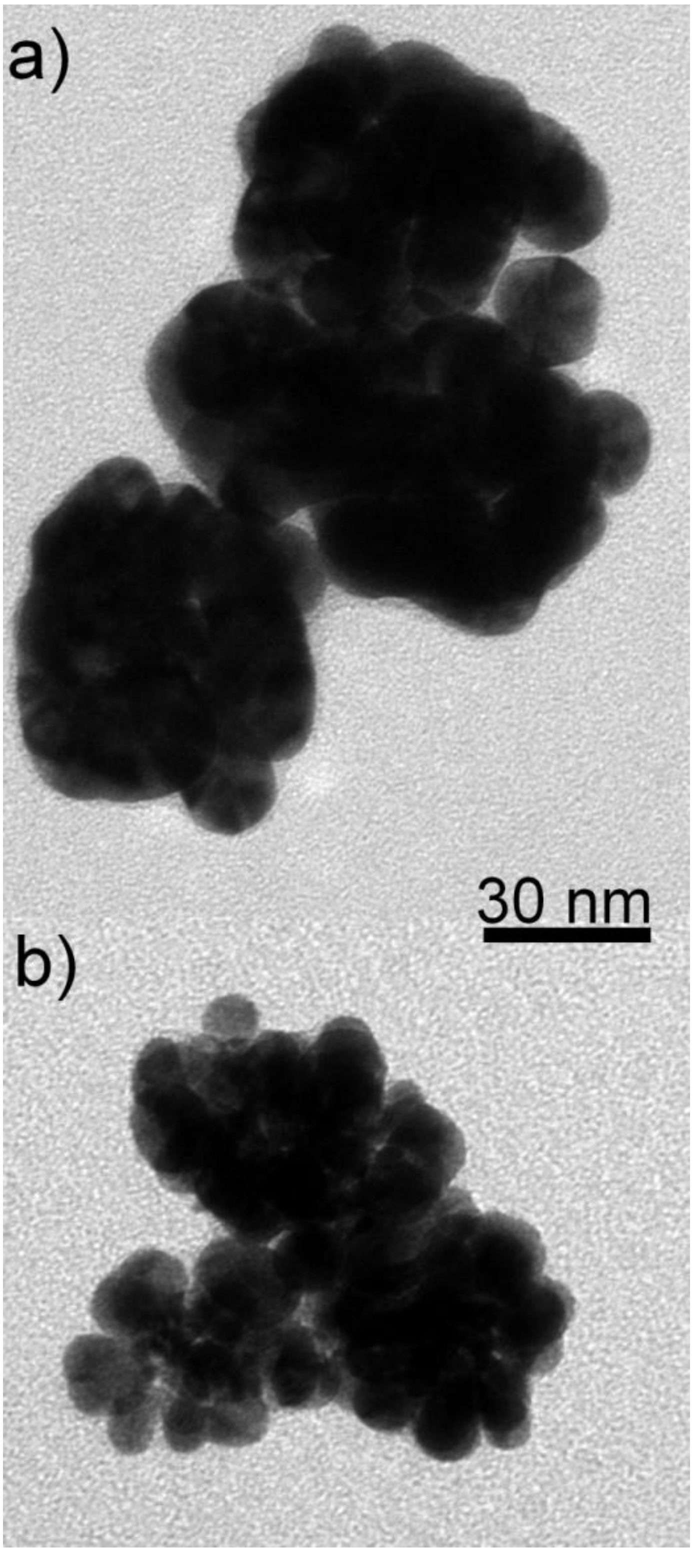

Fig. S10: TEM images of Pt@Au core-satellite structures prepared with the addition of: a) 100 µl and b) 400 µl of a ‘medium-compact’ Pt dendrite stock solution.

Table S2: Amount of Pt dendrites used for the synthesis of Pt@Au core-satellite structures an d sizes of the nanostructures obtained.

Quantity of Pt NDs	**Size of Pt@Au core satellite NPs**
100 µl	61 nm
200 µl	57 nm
400 µl	47 nm

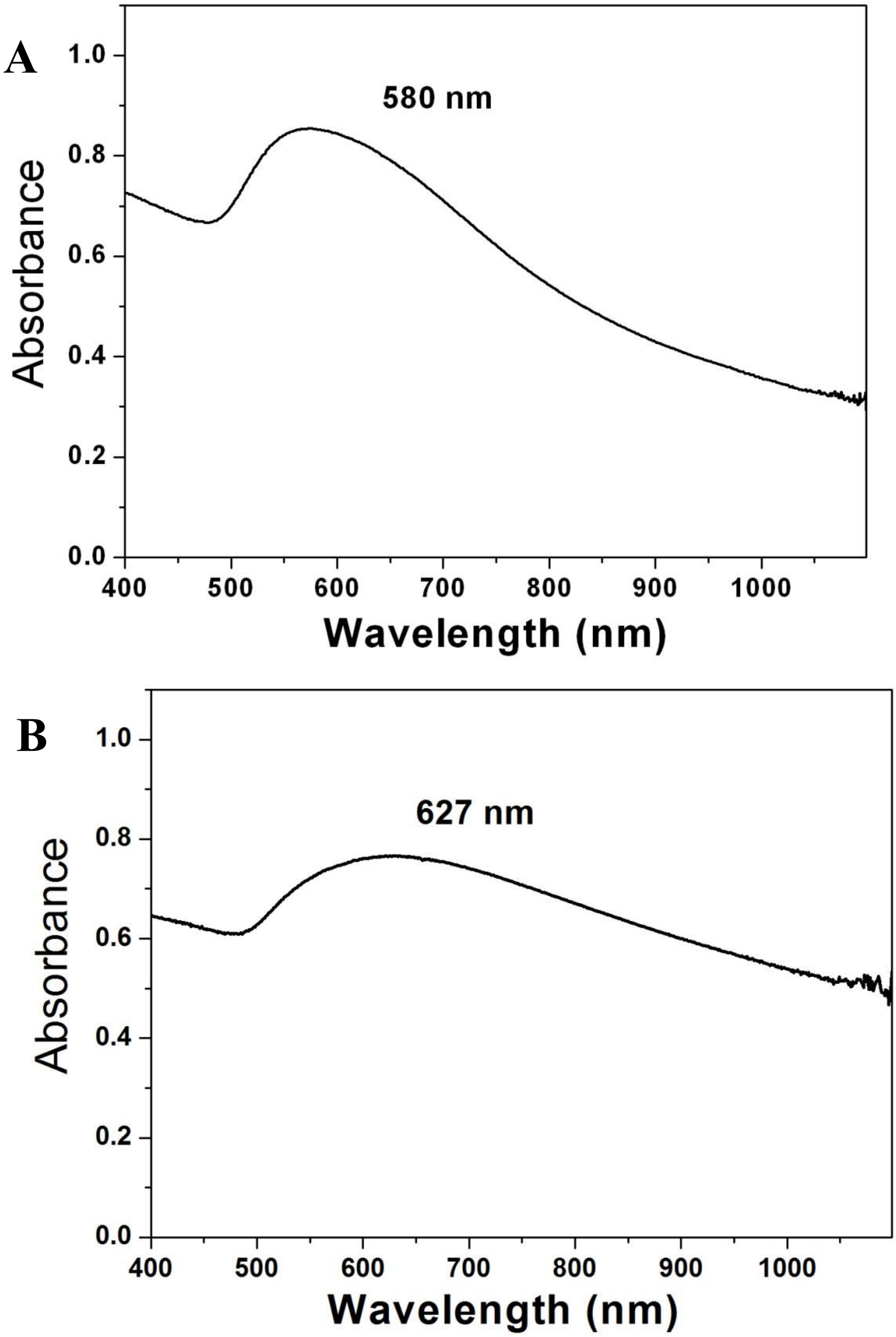

Fig. S11: Vis-NIR extinction spectrum of an aqueous dispersion of Pt@Au core-satellite nanostructure with an overall average size of ~ 57 nm (A) and 61 nm (B).

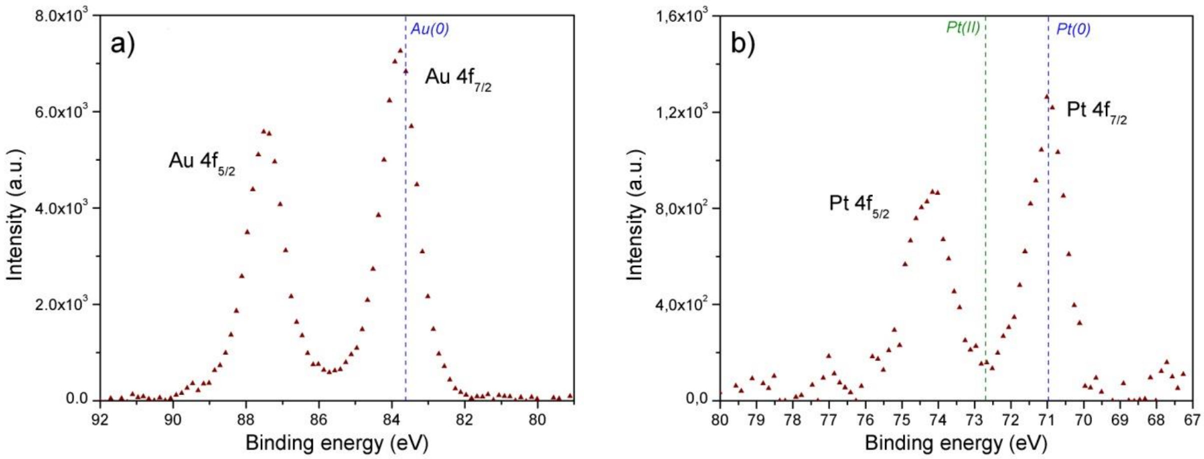

Fig. S12. High resolution XPS spectra for Au4f (a) and Pt4f (b) regions of Pt@Au core-satellite shown at Fig. 3 in the main manuscript.

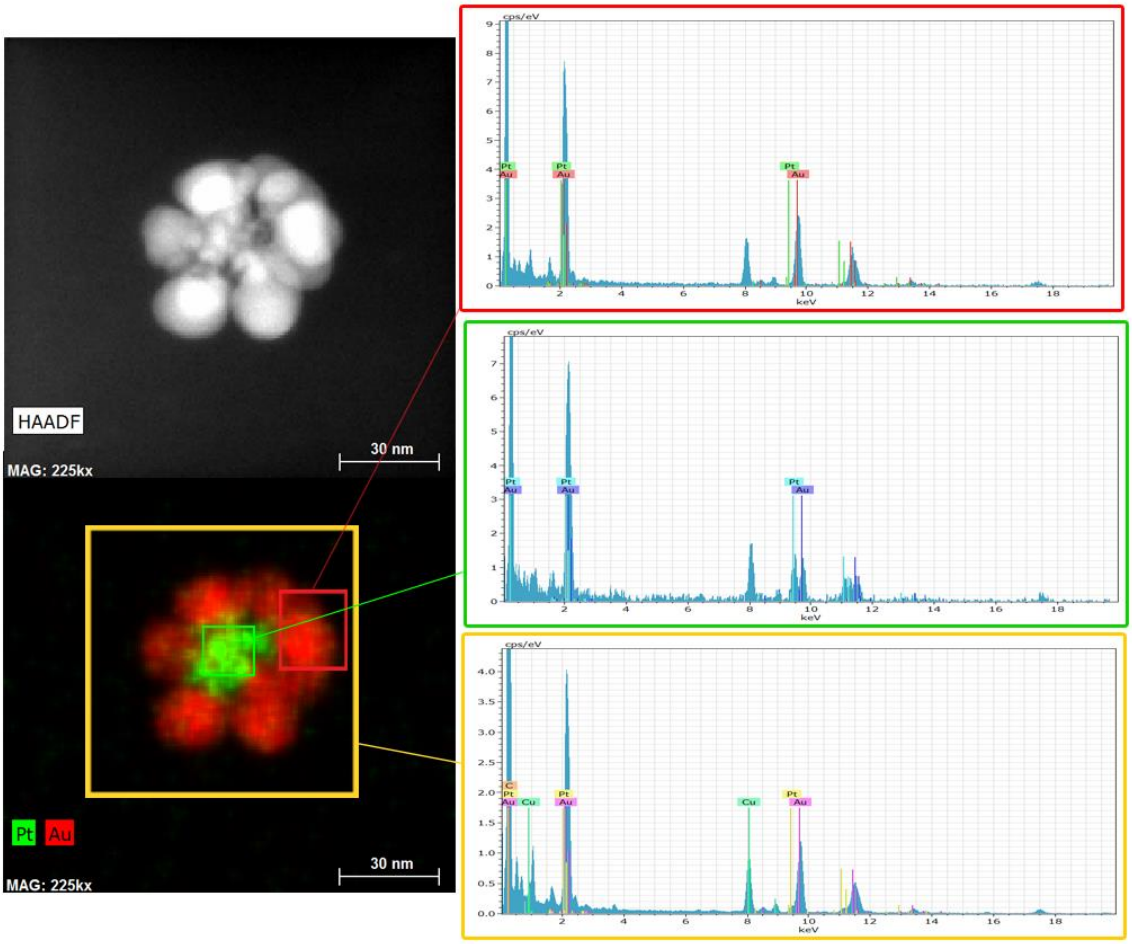

Fig. S13: HAADF image, EDX map and relative spectra of a Pt@Au core-satellite particle.

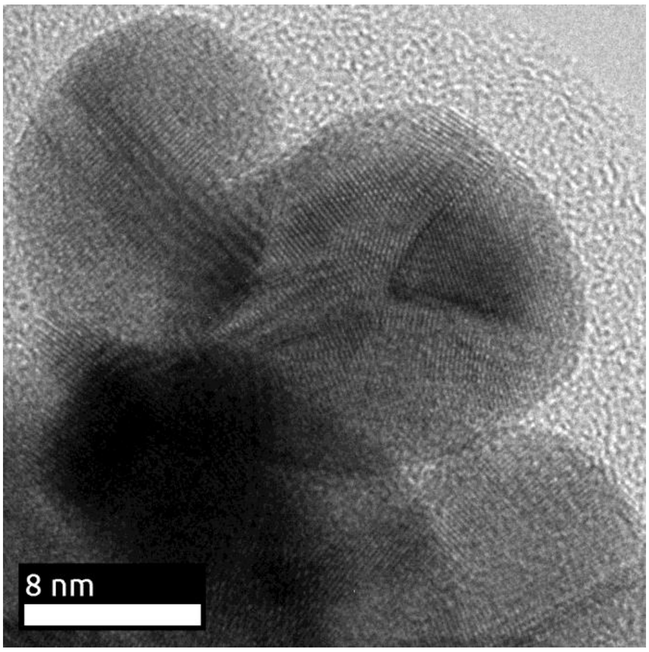

Fig. S14: HRTEM image of one of the Au 'petals' surrounding a Pt dendrite in a Pt@Au core-satellite structure: Twinning is always present.

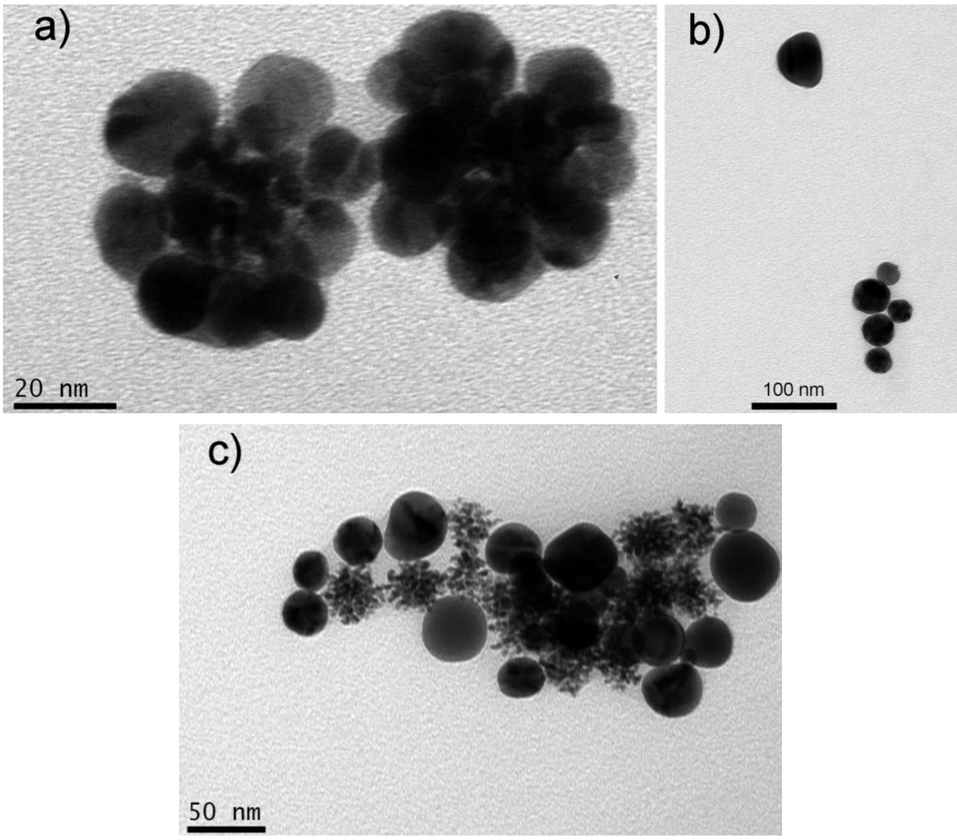

Fig. S15: TEM images of PVP-capped Pt-Au structures prepared by adding 200 μl of a Pt nanodendrite solution. The addition sequence of Au and Pt was: a) Pt first, Au last and b-c) Au first, Pt last. The addition of Au salt before the Pt seeds gives rise to free Au nanoparticles.

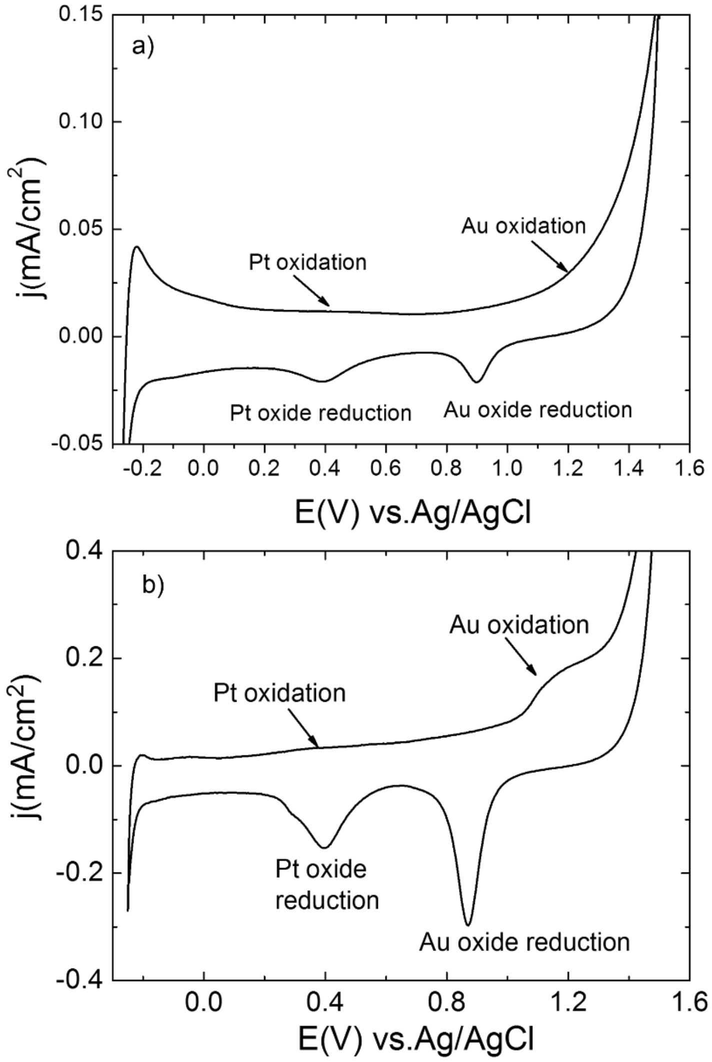

Fig. S16. Cyclic voltammograms recorded at glassy carbon (GC) electrodes modified with (a) Pt-Au dimers (GC-Pt-Au) and (b) Pt@Au core-satellite nanoparticles (GC-Pt@Au) in 0.1 M $HClO_4$. Scan rate 50 mV/s.

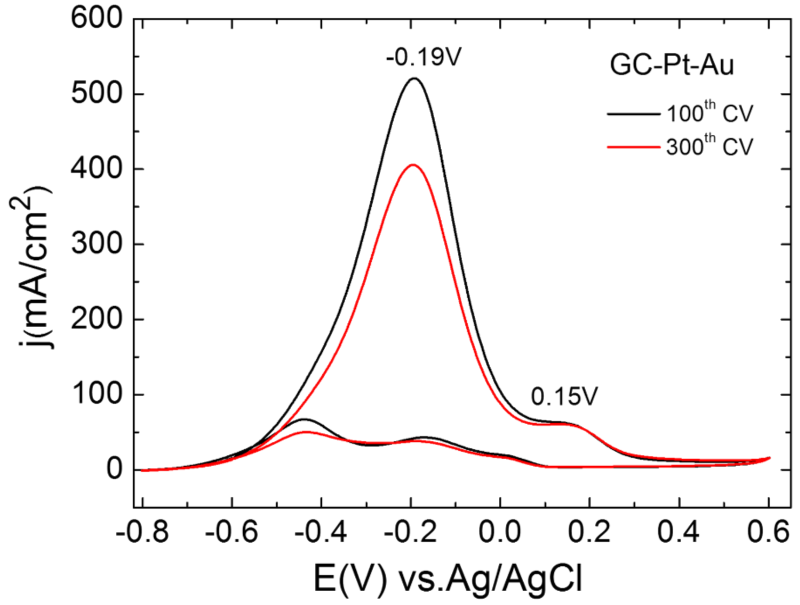

Fig. S17. Catalytic activity of Pt-Au dimer for EOR as a function of number of CVs. Scan rate 50 mV/s. The electrolyte aqueous solution contained 1M Ethanol and 1M NaOH.

The Pt-Au catalysts display a better catalytic activity for EOR as compared to its Pt nanodendrite (see reference **S1**) and spherical gold nanoparticle (**Fig. S20**) counterparts.

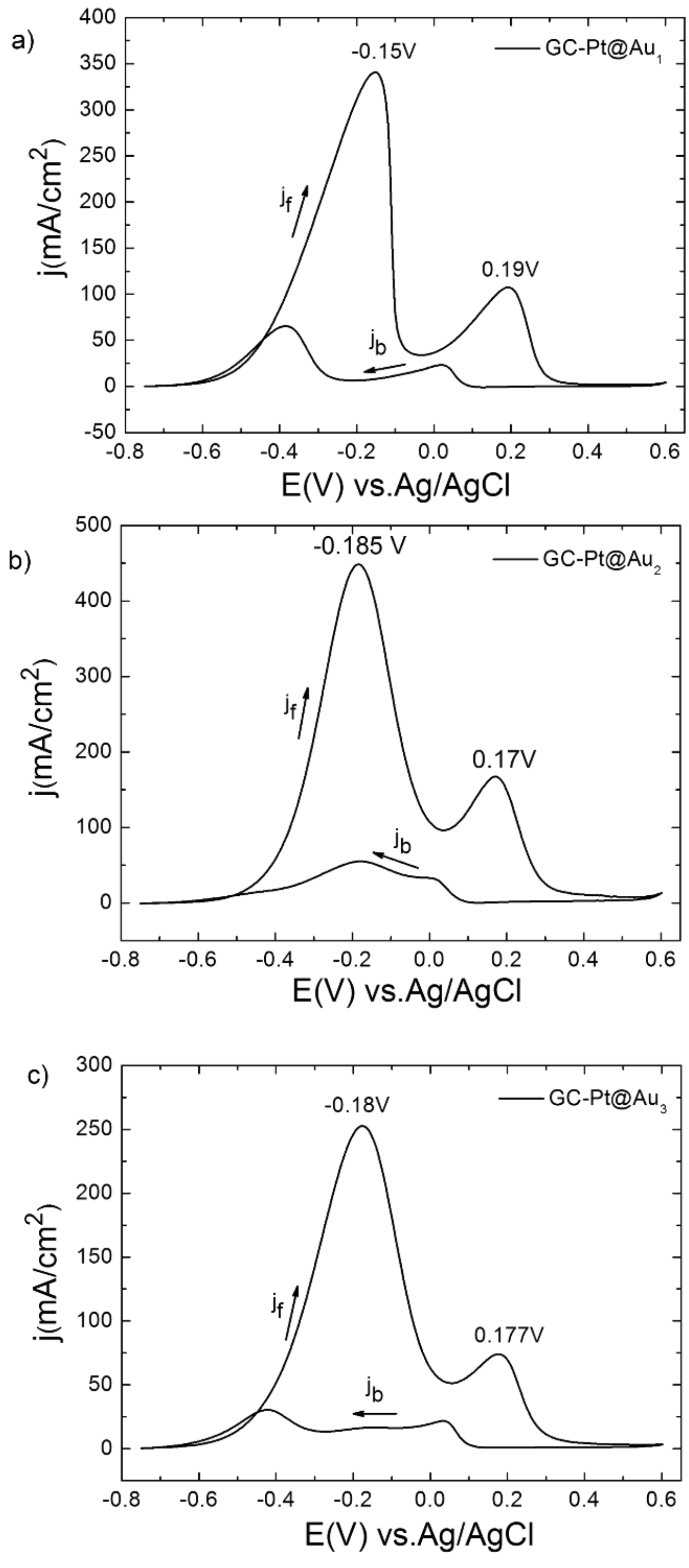

Fig. S18. Cyclic voltammograms recorded in 1 M ethanol and 1 M NaOH at glassy carbon (GC) electrodes modified with Pt@Au core satellite particles: a) GC-Pt@Au_1, Au size ~13 nm, GC-Pt@Au_2, Au size ~17.5 nm and GC-Pt@Au_3, Au size ~20 nm. Scan rate 50 mV/s.

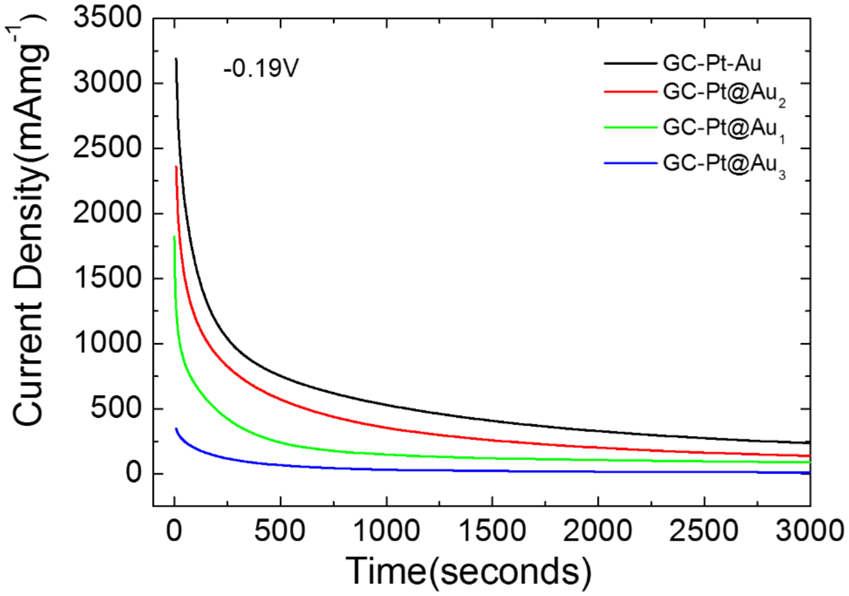

Fig. S19. Chronoamperograms measured at GC-Pt-Au dimer (black line) and GC-Pt@Au core-satellite (red, green and blue lines) modified electrodes at -0.19 V in 1 M ethanol and 1 M NaOH aqueous solution.

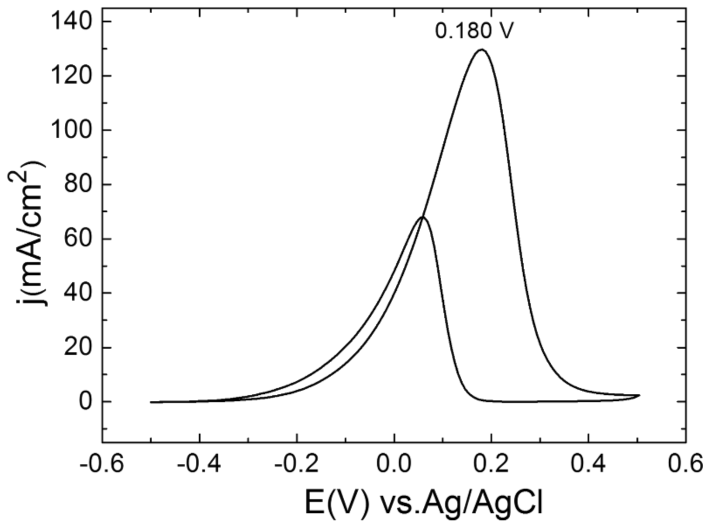

Fig. S20. Ethanol oxidation reaction recorded at glassy carbon (GC) electrodes modified with 15 nm PVP-stabilized Au nanoparticles in 1 M ethanol and 1 M NaOH. Scan rate 50 mV/s.

Table S3. Specific parameters for EOR performed at GC modified electrodes in 1 M ethanol and 1 M NaOH.

GC—modified electrodes	Current densities(mA/cm^2)	Scan rate (mVs^{-1})	Final product	Peak Potential[b] (acetaldehyde formation) (V)	Peak Potential[b] (CO_2 production) (V)
GC-Pt-Au	520.0	50	CO_2	0.15	-0.19
GC-Pt@Au$_1$ (47 nm)	340.6	50	CO_2	0.19	-0.15
GC-Pt@Au$_2$ (57 nm)	448.5	50	CO_2	0.17	-0.185
GC-Pt@Au$_3$ (61 nm)	252.6	50	CO_2	0.177	-0.18
GC-Pt porous[a]	197.0	50	CO_2	0.054	-0.26
GC-Pt medium compact[a]	61.0	50	CO_2	0.056	-0.26
GC-Au	129.0	50	Acetalde-hyde	0.180	no peak

a. The data was taken from reference [S1]

b. V vs. Ag-AgCl

REFERENCES

S1) Mourdikoudis, S.; Chirea, M.; Altantzis, T.; Pastoriza-Santos, I.; Pérez-Juste, J.; Silva, F.; Bals, S.; Liz-Marzán, L. M. *Nanoscale* **2013**, *5*, 4776.

Supporting Movie Legends Movies

Movies showing the 3D reconstruction of an Au-Pt dimer (Movie S1) and Pt@Au core-satellites (Movies S2-S5) obtained using electron tomography.